AMERICAN SOCIETY FOR MICROBIOLOGY | Molecular and Cellular Biology®

RESEARCH ARTICLE

Transient Overexpression of Vascular Endothelial Growth Factor A in Adipose Tissue Promotes Energy Expenditure via Activation of the Sympathetic Nervous System

Yueshui Zhao,[a,b] Xin Li,[a] Li Yang,[a] Kristin Eckel-Mahan,[a] Qingchun Tong,[a] Xue Gu,[a,c] Mikhail G. Kolonin,[a] Kai Sun[a]

[a]Center for Metabolic and Degenerative Diseases, The Brown Foundation Institute of Molecular Medicine for the Prevention of Human Diseases, University of Texas Health Science Center at Houston, Houston, Texas, USA

[b]Laboratory of Molecular Pharmacology, Department of Pharmacology, School of Pharmacy, Southwest Medical University, Luzhou, Sichuan, China

[c]Center for Precision Environmental Health, Baylor College of Medicine, Houston, Texas, USA

ABSTRACT Adipose-derived vascular endothelial growth factor A (VEGF-A) stimulates functional blood vessel formation in obese fat pads, which in turn facilitates healthy expansion of the adipose tissue. However, the detailed mechanism(s) governing the process remains largely unknown. Here, we investigated the role of sympathetic nervous system activation in the process. To this end, we induced overexpression of VEGF-A in an adipose tissue-specific doxycycline (Dox)-inducible transgenic mouse model for a short period of time during high-fat diet (HFD) feeding. We found that local overexpression of VEGF-A in adipose tissue stimulated lipolysis and browning rapidly after Dox induction. Immunofluorescence staining against tyrosine hydroxylase (TH) indicated higher levels of sympathetic innervation in adipose tissue of transgenic mice. In response to an increased norepinephrine (NE) level, expression of β3-adrenoceptor was significantly upregulated, and the downstream protein kinase A (PKA) pathway was activated, as indicated by enhanced phosphorylation of whole PKA substrates, in particular, the hormone-sensitive lipase (HSL) in adipocytes. As a result, the adipose tissue exhibited increased lipolysis, browning, and energy expenditure. Importantly, all of these effects were abolished upon treatment with the β3-adrenoceptor antagonist SR59230A. Collectively, these results demonstrate that transient overexpressed VEGF-A activates the sympathetic nervous system, which hence promotes lipolysis and browning in adipose tissue.

KEYWORDS VEGF-A, β3-adrenoceptor, browning, energy expenditure, lipolysis, sympathetic activation

Obesity, characterized by an excess of white adipose tissue (WAT), is a major risk factor for many chronic disorders, including type 2 diabetes, cardiovascular diseases (CVD), and hypertension (1–3). Adipose tissue (AT) has the ability for lifelong growth and almost unlimited expansion. Adipocyte differentiation and adipose tissue growth rely on the formation of new blood vessels that support proper oxygen, nutrition, and stem and precursor cells (3). However, during obesity development, the synchrony between adipose tissue expansion and vascularization is lost, giving rise to a local hypoxic condition (1, 4–6), which further results in fibrosis, inflammation, and systemic metabolic disorders, such as insulin resistance and atherosclerosis (4, 5, 7, 8). Hence, improving the vascular network and reversing hypoxia in the pathologically expanded WAT by angiogenesis have been proposed to be a potential strategy to deal with obesity and obesity-related metabolic disorders (2–4, 6).

Multiple angiogenic factors, such as vascular endothelial, hepatocyte, and fibro-

Received 15 May 2018 **Returned for modification** 29 May 2018 **Accepted** 14 August 2018

Accepted manuscript posted online 20 August 2018

Citation Zhao Y, Li X, Yang L, Eckel-Mahan K, Tong Q, Gu X, Kolonin MG, Sun K. 2018. Transient overexpression of vascular endothelial growth factor A in adipose tissue promotes energy expenditure via activation of the sympathetic nervous system. Mol Cell Biol 38:e00242-18. https://doi.org/10.1128/MCB.00242-18.

Copyright © 2018 American Society for Microbiology. All Rights Reserved.

Address correspondence to Kai Sun, kai.sun@uth.tmc.edu.

Y.Z. and X.L. contributed equally to this article.

blast growth factors (VEGF, HGF, and FGF, respectively) as well as angiopoietin 1 (Ang-1) and Ang-2 are secreted by adipocytes, suggesting that they autoregulate vascular homeostasis (3). Among them, VEGF-A is the only bona fide endothelial cell growth factor that has been found to account for most of the proangiogenic activity in adipose tissue (9, 10). VEGF-A levels in adipose tissue are significantly upregulated after exercise and cold exposure (11, 12). However, adipose tissue frequently fails to mount high enough levels of VEGF-A in response to hypoxia in obese adipose tissue, which leads to a lack of angiogenesis in obese adipose tissue (5). Interestingly, we recently applied a doxycycline (Dox)-inducible mouse model that specifically overexpresses VEGF-A in adipose tissue and found that locally overexpressed VEGF-A stimulated functional new blood vessels by angiogenesis. We further demonstrated that long-term angiogenesis facilitated adipose tissue expansion by reducing the local hypoxia, fibrosis, and inflammation (13, 14). As a result, the mice remained metabolically fit under a high-fat diet (HFD), with enhanced energy expenditure and improved insulin sensitivity (13, 14). Of note, among all the metabolically beneficial effects of VEGF-A in obese adipose tissue, the most significant one is a higher rate of energy expenditure (14, 15). As a result, the VEGF-A transgenic (Tg) mice gained less body weight despite unchanged food intake (15). Importantly, we previously found that under HFD challenge, overexpression of VEGF-A resulted in features characteristic of brown (beige) adipocytes in subcutaneous WAT (sWAT) of VEGF-A Tg mice (14). Confirming sWAT browning, we observed elevated expression levels of brown-fat-associated proteins, including uncoupling protein 1 (UCP1), and peroxisome proliferator-activated receptor γ (PPARγ) coactivator 1α (PGC-1α) in sWAT (14). These findings were confirmed subsequently by other reports (11, 15, 16).

Because previous studies have focused on long-term VEGF-A effects, it has remained unclear if angiogenesis was responsible for WAT browning or whether VEGF-A has direct effects on other cells. To investigate short-term VEGF-A signaling in WAT, we took advantage of the Dox-inducible adipose tissue-specific VEGF-A transgenic mouse model that we previously reported (14). To determine the direct function of VEGF-A and rule out possible secondary effects during chronic obesity, in the current study we induced VEGF-A expression by Dox for only a short period of time (1 week) under HFD challenge. Surprisingly, even after short-term induction, VEGF-A triggered denser local sympathetic nerve fiber innervation, which further stimulated the upregulation of β3-adrenoceptor and the activation of the downstream protein kinase A (PKA) signaling pathway, ultimately leading to increased lipolysis and browning in adipose tissue. Thus, our results provide a greater understanding of the molecular mechanism by which VEGF-A stimulates adipose tissue activity to accelerate energy expenditure.

RESULTS

Transient overexpression of VEGF-A in adipose tissue reduces fat mass and increases energy expenditure after HFD feeding. Previously, we reported that adipose-derived VEGF-A in chronically HFD-challenged mice caused dramatically reduced fat mass size and body weight, which was associated with improved insulin sensitivity, as well as enhanced energy expenditure (14). Here, we challenged the VEGF-A Tg mice with an HFD plus 30 mg/kg Dox for only 7 days to rule out the potential secondary metabolic effects of chronic diet-induced obesity. To our surprise, even after the short-term induction, VEGF-A Tg mice gained less body weight and had smaller fat pads than their littermate controls (Fig. 1A to C). Moreover, histological examination revealed a smaller adipocyte size in WAT of VEGF-A Tg mice (Fig. 1D and E).

Indirect calorimetry showed that both the volume of O_2 consumption (VO_2) (Fig. 1F and G) and volume of CO_2 production (VCO_2) (Fig. 1I and J) were significantly increased in VEGF-A Tg mice, indicating higher energy turnover in these mice. CalR analysis further indicated that the differences in energy turnover are correlated to group effect but not to the body mass effect (Fig. 1H and K), suggesting that the energy expenditure effects are caused solely by inherent differences between the groups but not by a

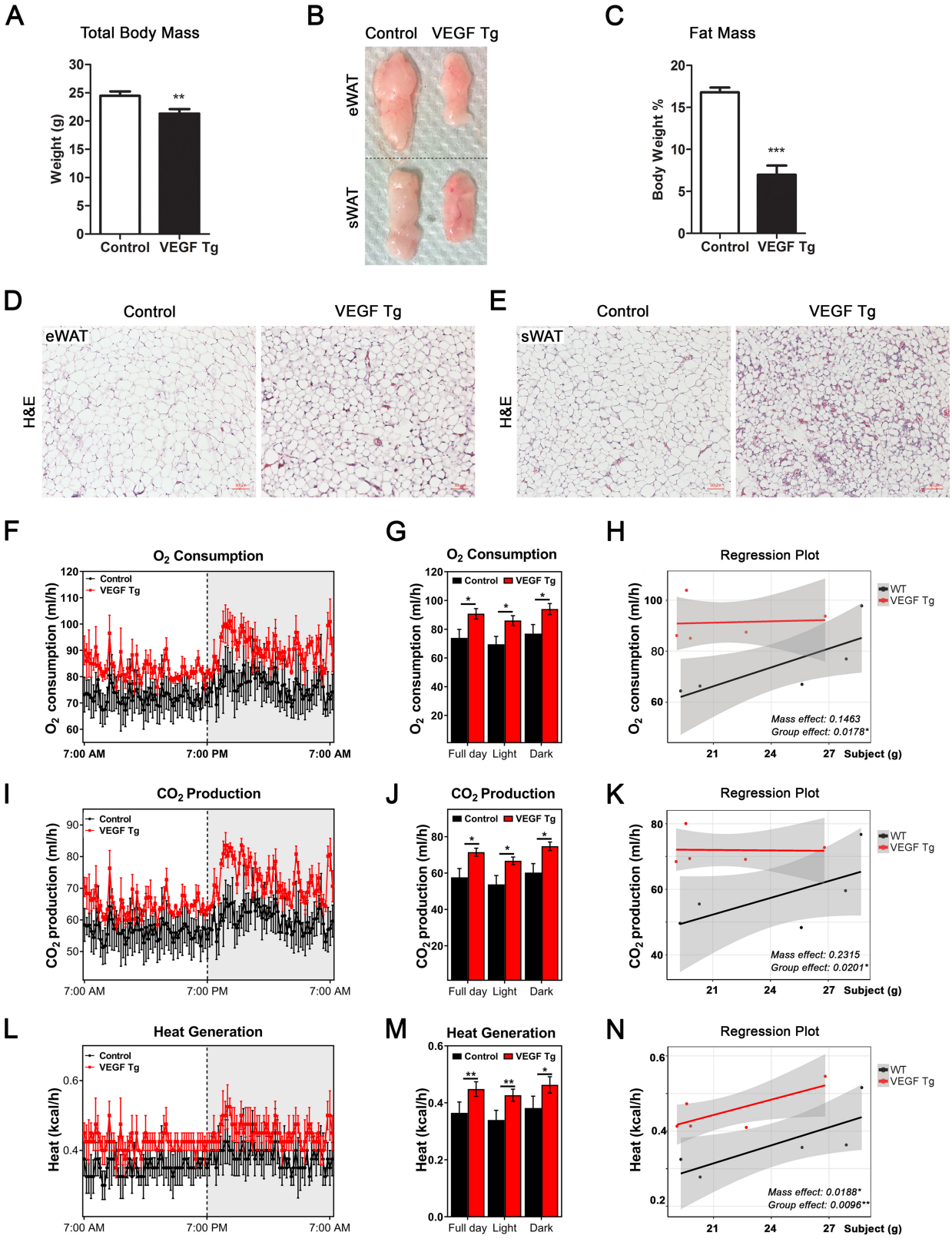

FIG 1 VEGF-A transgenic mice exhibit smaller adipocytes and reduced total fat mass shortly after VEGF-A induction. (A) Body weights of VEGF Tg mice and their littermate controls after feeding with an HFD (60% fat) plus 30 mg/kg Dox for 7 days ($n = 6$ per group; Student's t test, **, $P < 0.01$). (B) Comparison of the sizes of different adipose tissues (eWAT and sWAT) collected from VEGF Tg mice and their littermate controls after HFD-Dox feeding for 7 days. (C) MRI analysis of fat mass in VEGF Tg mice and their littermate controls after HFD-Dox feeding for 7 days ($n = 6$ per group; Student's t test, ***, $P < 0.001$). (D and E) H&E staining of eWAT and sWAT collected from VEGF Tg mice and their littermate controls after HFD-Dox feeding for 7 days (scale bar, 50 μm). (F to N) Indirect calorimetry performed in a CLAMS system after HFD-Dox feeding for 7 days. (F) O_2

(Continued on next page)

covariant body weight factor. The respiratory exchange ratio (RER) (VCO_2/VO_2) showed no difference between VEGF-A Tg mice and their littermate controls, indicating no change in glucose and lipid turnover rates between the two groups (data not shown). Importantly, heat generation was significantly increased in the VEGF-A Tg mice (Fig. 1L and M), suggesting that overexpressed VEGF-A in adipose tissue increases thermogenesis. Of note, CalR analysis indicated that the thermogenic effect is correlated not only with the group effect but also to the body mass effect (Fig. 1N).

In summary, the results suggested that short-term induction of VEGF-A in adipose tissue leads to lower body weights and a smaller fat mass as well as a higher rate of energy expenditure and an enhanced thermogenic effect, suggesting a direct local role of adipose VEGF-A in whole-body metabolism.

Local overexpression of VEGF-A in adipose tissue increases mitochondrial biogenesis and function. The mitochondrion is the predominant organelle for energy production in adipose tissues (17). To determine whether mitochondrial number and function are regulated by VEGF-A in adipose tissue, we first measured β-oxidation-related gene expression and found that most of this group of genes were significantly upregulated in sWAT of the VEGF-A Tg mice (Fig. 2A). We then examined the effect of VEGF-A overexpression on mitochondrial biogenesis. Analysis of mitochondrial biogenesis gene expression revealed that the *Pgc1α*, *Nrf1*, and CoxIV genes were all upregulated in the sWAT of the VEGF-A Tg mice (Fig. 2B). The levels of mitochondrial DNA (so-called mtDNA) were significantly higher (Fig. 2C), further supporting the increase in mitochondrial content in the sWAT of the VEGF-A Tg mice. In line with the quantitative PCR (qPCR) and mtDNA results, immunofluorescence staining (IF) with an antibody to CoxIV, the biomarker of mitochondria, showed that the positive green fluorescent signals were much stronger in the sWAT of the VEGF-A Tg mice (Fig. 2E). Furthermore, Western blotting using an antibody against succinate dehydrogenase subunit A (SDHA), another mitochondrial protein, indicated more SDHA proteins in the sWAT of the VEGF-A Tg mice (Fig. 2F).

We then measured the function of mitochondria in the adipose tissue of the VEGF-A Tg mice by Seahorse XFe24 assay. Fat pads collected from VEGF-A Tg mice consistently exhibited a higher oxygen consumption rate (OCR) than the controls at different time points upon treatment with different compound (Fig. 2G). In all, our results clearly show that mitochondrial content and function were increased in the sWAT of the VEGF-A Tg mice. Future studies on isolated mitochondria are required to further confirm the enhanced mitochondrial function.

Local overexpression of VEGF-A in adipose tissue results in enhanced lipolysis. Previously, we along with others reported that VEGF-A promotes adipocyte browning, manifested as multilocular lipid droplets in sWAT (11, 14, 18). Here, we further found that in addition to UCP1-positive staining by immunohistochemistry (IHC) with anti-UCP1 antibody (Fig. 2D) and the multilocular structures, the sWAT of the transgenic mice showed smaller lipid droplets (Fig. 1D). Since the balance between lipid synthesis (lipogenesis) and lipid breakdown (lipolysis) determines the total lipid levels in adipocytes (19), we next analyzed the expression levels of key enzymes involved in these processes. The qPCR results revealed that the levels of genes for lipogenic enzymes, i.e., fatty acid synthase (*Fasn*) and acetyl coenzyme A (acetyl-CoA) carboxylase 1 (AccI), were dramatically downregulated (Fig. 3A), while the levels of genes for the lipolytic enzymes, i.e., adipose triglyceride lipase (*Atgl*), hormone-sensitive lipase (*Hsl*), and lipase

FIG 1 Legend (Continued)
consumption profile of VEGF Tg and control mice during a 12-h light-dark cycle. (G) Histogram representative of full-day and light and dark periods of the results shown in panel F. (H) General linear model-based regression plot of the association between O_2 consumption and mass (grams) as well as the association between O_2 consumption and the group factor. (I) CO_2 production profile of VEGF Tg and control mice during a 12-h light-dark cycle. (J) Histogram representative of full day and light and dark periods of the results shown in panel I. (K) General linear model-based regression plot of the association between CO_2 production and mass as well as the association between CO_2 production and the group factor. (L) Heat generation profile of VEGF Tg and control mice during a 12-h light-dark cycle. (M) Histogram representative of full day and light and dark periods of the results shown in panel L. (N) General linear model-based regression plot of the association between heat generation and mass as well as the association between heat generation and the group factor. ($n = 5$ per group; ANCOVA test, *, $P < 0.05$; **, $P < 0.01$).

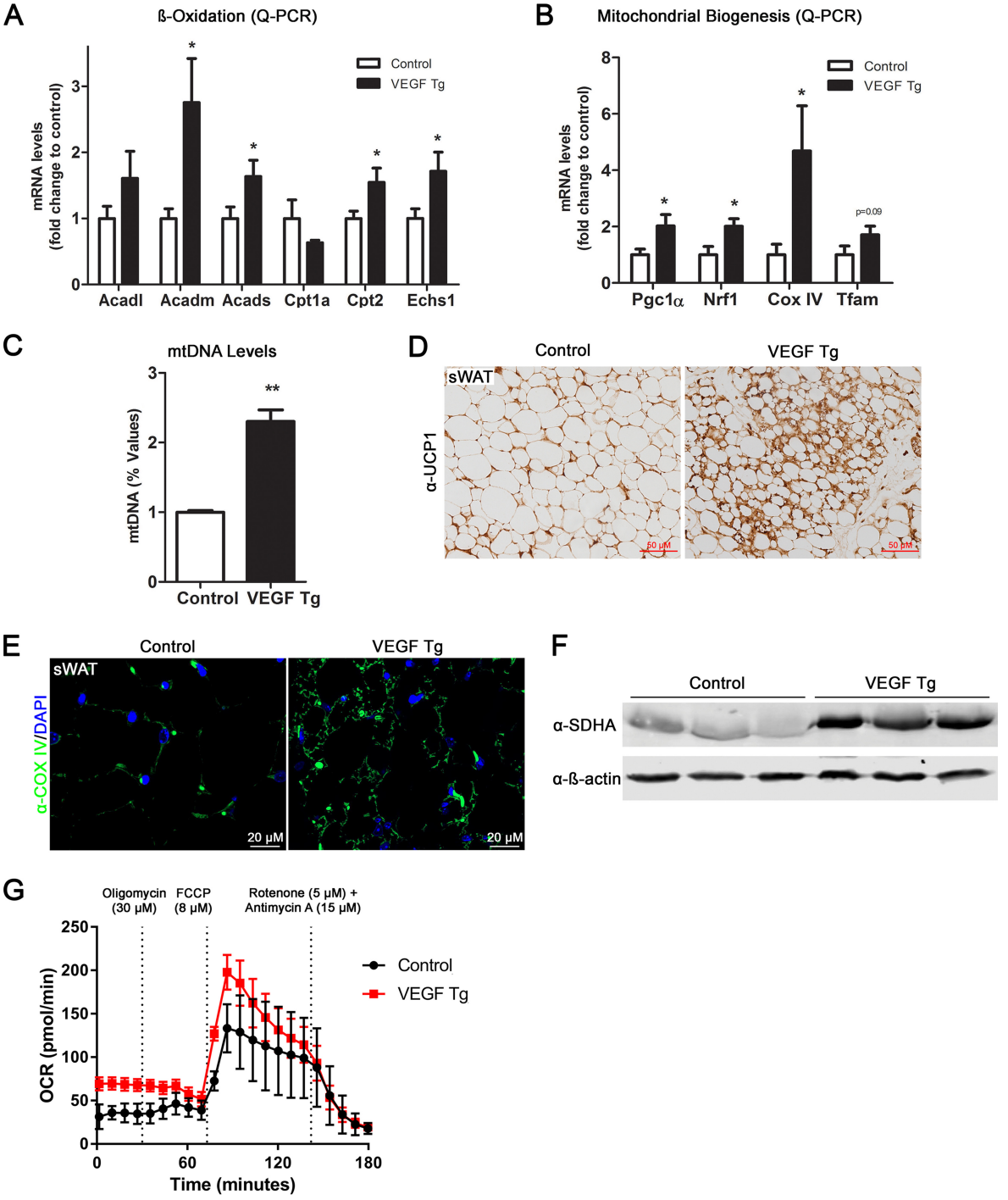

FIG 2 Local overexpression of VEGF-A stimulates mitochondrial biogenesis and functions in adipose tissues. (A) qPCR analysis of β-oxidation-related genes, namely, *Acadl*, *Acadm*, *Acads*, *Cpt1a*, *Cpt2*, and *Echs1*, in sWAT of VEGF Tg mice and their littermate controls after HFD-Dox feeding for 7 days ($n = 5$ per group; Student's *t* test, *, $P < 0.05$). (B) qPCR analysis of mitochondrial biogenetic genes including the *Pgc1α*, *Nrf1*, CoxIV, and *Tfam* genes in sWAT of VEGF Tg mice and their littermate controls after HFD-Dox feeding for 7 days ($n = 5$ per group; Student's *t* test, *, $P < 0.05$). (C) The mitochondrial DNA (mtDNA) content in sWAT of VEGF Tg mice and their littermate controls after HFD-Dox feeding for 7 days. The copy number of mtDNA was calculated by the ratio of the mtDNA gene for NADH dehydrogenase alpha 1 (*Nadha1*) to the nuclear gene for lipoprotein lipase (*Lpl*) ($n = 5$ per group; Student's *t* test, **, $P < 0.01$). (D) IHC staining with anti-UCP1 antibody in sWAT of VEGF Tg mice and their littermate controls after HFD-Dox feeding for 7 days (scale bar, 50 μm). (E) Immunofluorescence (IF) staining with anti-Cox IV antibody (green) in sWAT of VEGF Tg mice and their littermate controls after HFD-Dox feeding for 7 days. The nuclei were stained with DAPI (blue). (F) Western blotting of protein levels of SDHA with anti-SDHA antibody in sWAT of VEGF Tg mice and their littermate controls after HFD-Dox feeding for 7 days. Equal loading control was demonstrated by anti-β-actin antibody ($n = 3$ per group). (G) Oxygen consumption rate (OCR) in sWAT measured by a Seahorse XFe24 instrument. The sWAT was collected from VEGF Tg mice and their littermate controls after HFD-Dox feeding for 7 days. The injection time point and final concentration of different compounds used for mitochondrial stress assay are indicated in the panel ($n = 5$ per group).

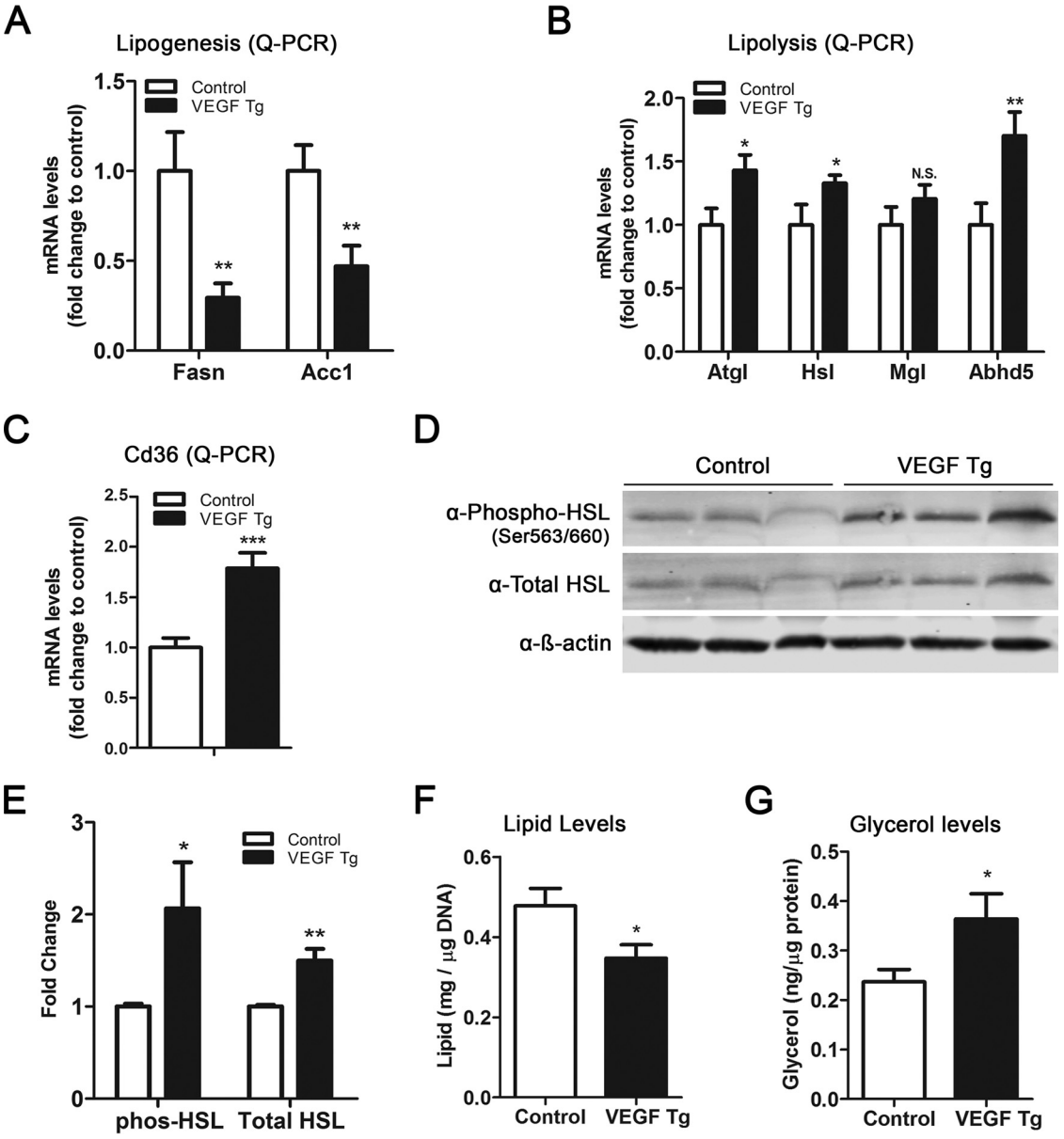

FIG 3 Local overexpression of VEGF-A stimulates lipolysis in sWAT. (A) qPCR analysis of lipogenic genes, namely, *Fasn* and *Accl*, in sWAT of VEGF Tg mice and their littermate controls after HFD-Dox feeding for 7 days ($n = 6$ per group; Student's *t* test, **, $P < 0.01$). (B) qPCR analysis of lipolytic genes, namely, *Atgl*, *Hsl*, *Mgl*, and *Abhd5*, in sWAT of VEGF Tg mice and their littermate controls after HFD-Dox feeding for 7 days ($n = 6$ per group; Student's *t* test, *, $P < 0.05$; **, $P < 0.01$, N.S., not significant). (C) qPCR analysis of the *Cd36* gene in sWAT of VEGF Tg mice and their littermate controls after HFD-Dox feeding for 7 days ($n = 6$ per group; Student's *t* test, ***, $P < 0.001$). (D and E) Western blotting and quantitative measurement of band density on the Western blots by ImageJ software for phosphorylated HSL (phos-HSL) at serine 563/660 as well as total HSL levels in sWAT of VEGF Tg mice and their littermate controls after HFD-Dox feeding for 7 days. Results were normalized by β-actin ($n = 3$ per group; Student's *t* test, *, $P < 0.05$; **, $P < 0.01$). (F) Total triglyceride content in sWAT of VEGF Tg mice and their littermate controls after HFD-Dox feeding for 7 days. ($n = 4$ per group; Student's *t* test, *, $P < 0.05$). (G) Glycerol levels (as the product of lipolysis) in sWAT of VEGF Tg mice and their littermate controls after HFD-Dox feeding for 7 days ($n = 4$ per group; Student's *t* test, *, $P < 0.05$).

cofactor α/β hydrolase domain-containing protein 5 (*Abhd5*, also known as *CGI-58*), were significantly upregulated in the sWAT of VEGF-A Tg mice (Fig. 3B). Of note, the mRNA levels of *CD36*, the key fatty acid transporter in adipose tissue (20), were also significantly upregulated in the sWAT of VEGF-A Tg mice (Fig. 3C).

In line with the upregulation of mRNA levels of the lipolytic genes, Western blotting results indicated that the total protein levels of hormone-sensitive lipase (HSL), a rate-limiting enzyme during lipolysis (21), were increased in the sWAT of VEGF-A Tg

mice. Importantly, the levels of phosphorylated HSL (a marker of VEGF-A activity) were also significantly increased (Fig. 3D and E), suggesting that the function of HSL was enhanced in the WAT of the VEGF-A Tg mice. Consequently, we observed that the total triglyceride levels were decreased, while the levels of glycerol, a product of the lipolytic process, were dramatically increased (Fig. 3F and G). We further measured lipolysis in epididymal WAT (eWAT) of the VEGF-A Tg mice, and we observed only milder effects than in sWAT (data not shown). Collectively, our results suggest that adipose-derived VEGF-A triggers enhanced lipolysis in WAT.

Local overexpression of VEGF-A in adipose tissue stimulates sympathetic neuronal innervation and activation. Next, we sought to investigate the mechanism(s) governing the browning and lipolytic effects induced by VEGF-A. Since sympathetic activation plays a critical role in browning and lipolysis in WAT (22–24), we thus determined whether overexpression of VEGF-A in adipose tissue stimulates local sympathetic activation. To this end, we first examined the nerve density by whole-mount IF with anti-tyrosine hydroxylase (anti-TH) antibody, the marker of the sympathetic neurons in the sWAT of the VEGF-A Tg mice and their littermate control mice. Interestingly, we found a dramatic increase in the density of the sympathetic nerve fibers in the sWAT of VEGF-A Tg mice upon Dox induction (Fig. 4A), suggesting an enhanced innervation in these adipose tissues. Of note, both the angiogenic and sympathetic innervation effects were not detected in the adipose tissues of the VEGF-A Tg mice without Dox treatment (data not shown). Furthermore, our previous study confirmed that there is no VEGF-A overexpression without Dox induction in the transgenic mice (14). We then analyzed several markers for the sympathetic nervous system (SNS) and found that the levels of norepinephrine (NE), the marker of innervated sympathetic neurons (22), were significantly higher in sWAT of the VEGF-A Tg mice (Fig. 4B, left). Importantly, the serum NE levels did not change between the groups (Fig. 4B, right), indicating the local innervation effect of VEGF-A.

Since NE triggers the downstream signaling events via the β3-adrenergic receptor (β3-AR; *Adrb3*) pathway (25), we next determined the expression levels of β3-AR and its counteracting partner, Adra2α, in the sWAT of VEGF-A Tg mice. As anticipated, the qPCR data indicated that the mRNA levels of β3-AR were significantly increased, whereas the levels of Adra2α were dramatically decreased in the sWAT of VEGF-A Tg mice (Fig. 4C). In line with the upregulation of β3-AR levels, the levels of cAMP as well as the levels of phosphorylated protein kinase A (PKA) substrates were also dramatically increased in sWAT of VEGF-A Tg mice (Fig. 4D and E), indicating the activation of the PKA pathway, the classical downstream event of stimulated sympathetic tone (26).

To determine the time course of angiogenesis and sympathetic innervation upon VEGF-A stimulation, we sacrificed the VEGF-A transgenic mice at different time points after Dox induction and performed IF costaining with antiendomucin and anti-TH on sWAT of the mice. Surprisingly, shortly after 1 day of Dox induction, both the blood vessel and sympathetic nerve fiber densities were dramatically increased, and the effects were significantly enhanced after 7 days of Dox induction (Fig. 4F). Interestingly, the newly formed blood vessels did not show colocalization with the increased sympathetic nerve fibers (Fig. 4F, bottom). Consistent with our previous observation (18), UCP1 gene upregulation initiated from the second day after Dox induction (Fig. 4G), suggesting that the browning effect might be brought about by sympathetic innervation and angiogenesis in the sWAT of the VEGF-A Tg mice.

Since brown adipose tissue (BAT) is another metabolically active adipose tissue (24), we then examined the effects of overexpressed VEGF-A in this fat pad. Histological examination revealed smaller lipid droplets in the BAT of VEGF-A Tg mice (Fig. 5A, top). IHC results further showed increased UCP1 and total phosphorylated PKA substrates in the BAT of VEGF-A Tg mice (Fig. 5A, middle and bottom). We next tested sympathetic innervation in this fat pad. As anticipated, the density of the sympathetic nervous system was also enhanced in the BAT of VEGF-A Tg mice (Fig. 5B, middle). While the angiogenesis was also significantly increased (Fig. 5B, top), the newly formed blood

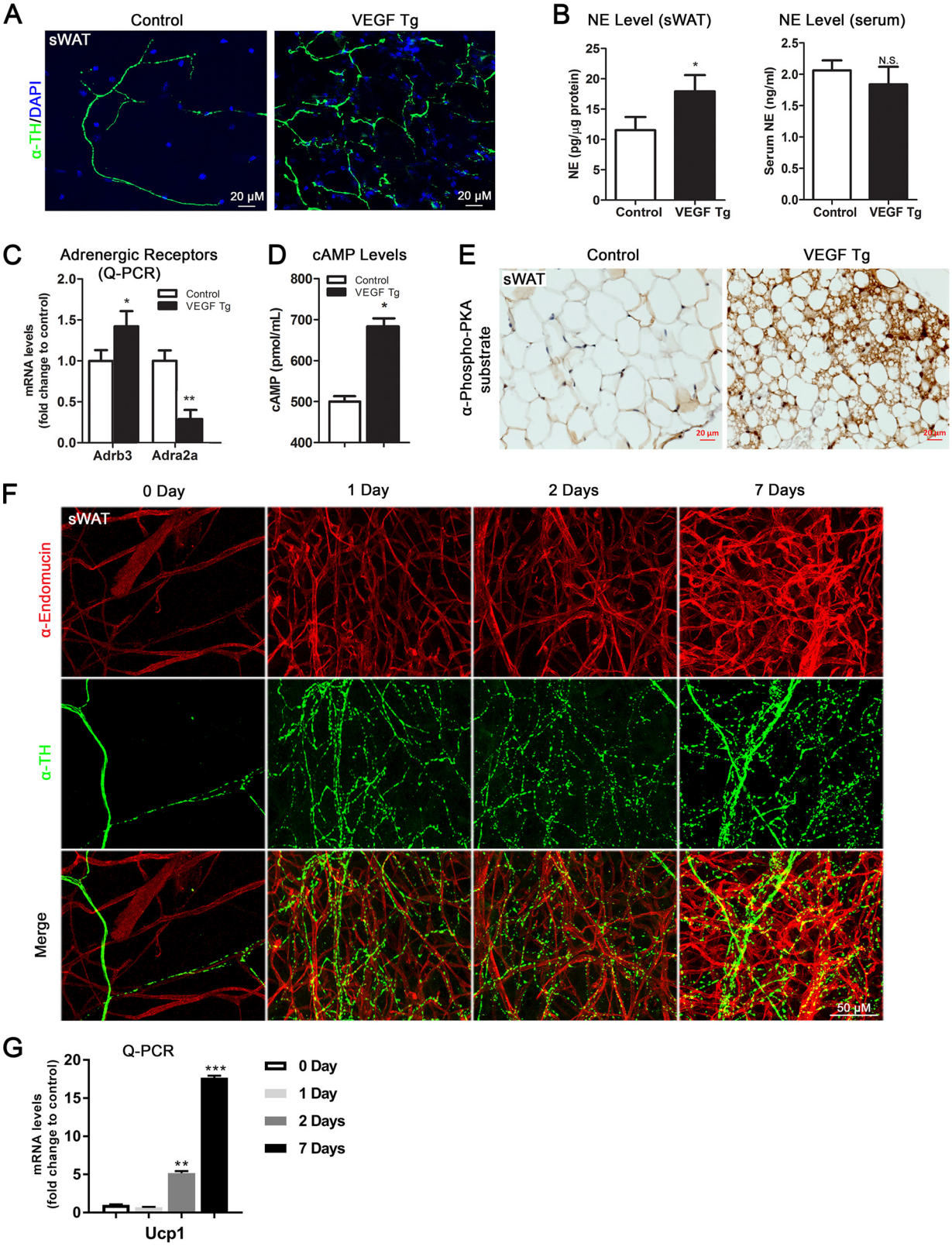

FIG 4 Local overexpression of VEGF-A induces sympathetic activation in sWAT. (A) Whole-mount IF staining with anti-tyrosine hydroxylase (α-TH) antibody (green) in sWAT of VEGF Tg mice and their littermate controls after HFD-Dox feeding for 7 days. The nuclei were stained with DAPI (blue). (B) NE levels in sWAT and serum of VEGF Tg mice and their littermate controls after HFD-Dox feeding for 7 days. Results for sWAT were normalized to the total protein levels ($n = 5$ for control group and $n = 6$ for VEGF Tg group; Student's t test, *, $P < 0.05$, N.S., not significant). (C) qPCR analysis of adrenergic receptor genes, namely, *Adrb3* and *Adra2a*, in sWAT of VEGF Tg mice and their littermate controls after HFD-Dox feeding for 7 days ($n = 6$ per group; Student's t test, *, $P < 0.05$; **, $P < 0.01$). (D) cAMP levels in sWAT of VEGF Tg mice and their littermate controls

(Continued on next page)

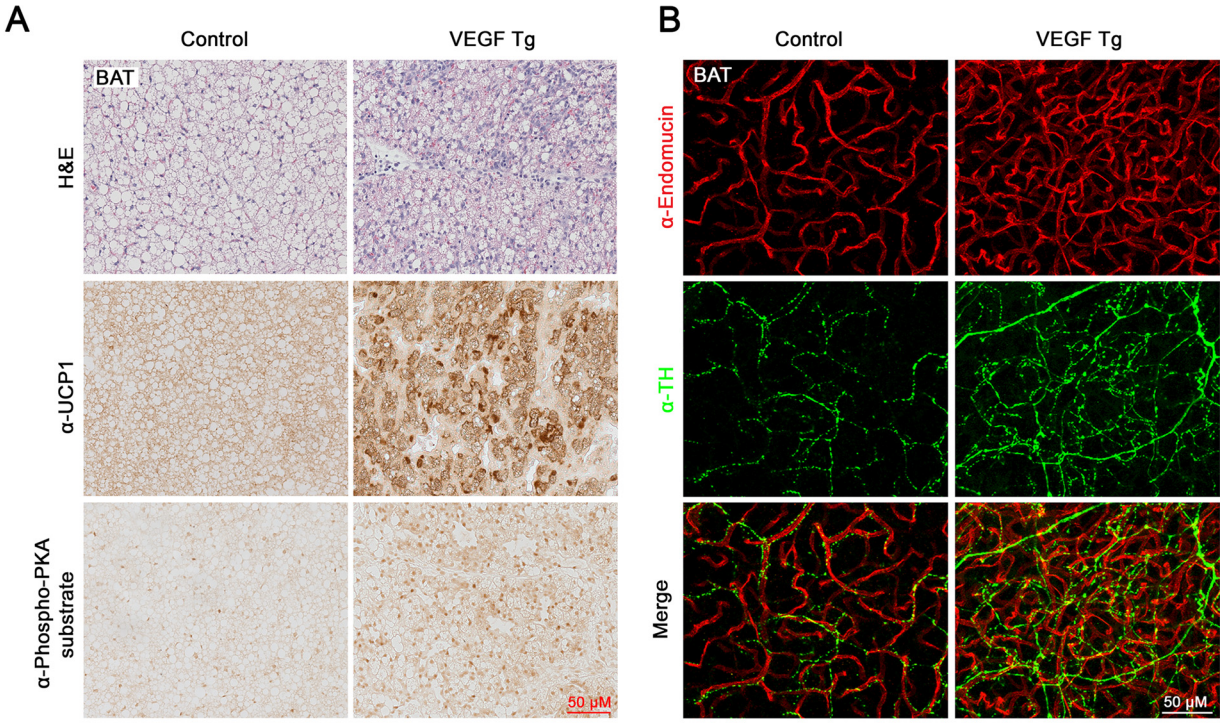

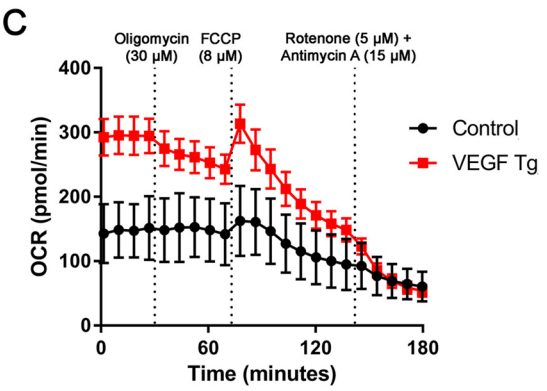

FIG 5 Local overexpression of VEGF-A induces sympathetic activation and increases mitochondrial functions in BAT. (A) H&E staining, IHC staining with anti-UCP1 antibody, and IHC staining with anti-phospho-PKA substrate antibody in BAT of VEGF Tg mice and their littermate controls after HFD-Dox feeding for 7 days (scale bar, 50 μm). (B) Whole-mount IF staining with antiendomucin antibody (red) and anti-tyrosine hydroxylase (α-TH) antibody (green) in BAT of VEGF Tg mice and their littermate controls after HFD-Dox feeding for 7 days (scale bar, 50 μm). (C) Oxygen consumption rate (OCR) in BAT measured by a Seahorse XFe24 analyzer. The BAT was collected from VEGF Tg and their littermate control mice after HFD-Dox feeding for 7 days. The injection time point and final concentrations of different compounds used for the mitochondrial stress assay are indicated in the panel ($n = 5$ per group).

vessels did not show colocalization with the increased sympathetic nerve fibers (Fig. 5B, bottom).

We also measured the function of mitochondria in the BAT of the VEGF-A Tg mice by Seahorse assay. Brown fat pads collected from VEGF-A Tg mice consistently exhibited a higher oxygen consumption rate (OCR) than the controls at different time points

FIG 4 Legend (Continued)
after HFD-Dox feeding for 7 days ($n = 5$ per group; Student's t test, *, $P < 0.05$). (E) IHC staining with anti-phospho-PKA substrate antibody in the sWAT of VEGF Tg mice and their littermate controls after HFD-Dox feeding for 7 days (scale bar, 20 μm). (F) Whole-mount IF staining with antiendomucin antibody (red) and anti-tyrosine hydroxylase (α-TH) antibody (green) in sWAT of VEGF Tg mice after HFD-Dox feeding for 0 days, 1 day, 2 days, and 7 days (scale bar, 50 μm). (G) qPCR analysis of *Ucp1* genes in sWAT of VEGF Tg mice after HFD-Dox feeding for 0 days, 1 day, 2 days, and 7 days ($n = 3$ per group; Student's t test, **, $P < 0.01$; ***, $P < 0.001$).

upon treatment with different compounds (Fig. 5C). Future studies on isolated mitochondria are required to further confirm the enhanced mitochondrial function.

Taken together, our results suggested that the sympathetic tone and its downstream β3-adrenergic signaling pathway are activated by VEGF-A in both the sWAT and BAT of the transgenic mice.

Adipose VEGF-A-induced metabolic effects are suppressed by β3-AR antagonist SR59230A. To further confirm the critical role of β3-AR signaling in VEGF-A-mediated metabolic improvements, we blocked the pathway by administrating the selective β3-AR antagonist SR59230A to the VEGF-A Tg and control mice by intraperitoneal (i.p.) injection. We found that after i.p. injection of SR59230A, cAMP levels induced by VEGF-A were dramatically reduced (Fig. 6A). To further determine the effect of SR59230A on PKA activity, we measured the total phosphorylated PKA substrates by IHC, and we found that the signals of the positive stains were dramatically suppressed upon SR59230A treatment (Fig. 6B, compare the right and middle panels). Histologically, we found that blockade of β3-AR by SR59230A enlarged the fat mass and the adipocyte size in the VEGF-A Tg mice (Fig. 6C and D). As anticipated, the lipolytic effect induced by VEGF-A was impaired by blockade of β3-AR, as shown by the downregulation of the critical lipolytic enzymes at both the mRNA and protein levels (Fig. 6E to G). Consequently, glycerol production induced by VEGF-A in sWAT was dramatically reduced after SR59230A treatment (Fig. 6H).

We then further determined the effects of the inhibitor on mitochondrial functions in the VEGF-A Tg mice. IHC staining using an antibody to UCP1 showed significantly decreased UCP1 in the sWAT of the VEGF-A Tg mice upon SR59230A treatment compared to levels in the controls (Fig. 7A, compare the right and middle panels), suggesting that the browning effect of VEGF-A was abolished by the blockage of β3-AR in the sWAT. This effect was further confirmed by qPCR analysis in which the mRNA levels of UCP1 were dramatically downregulated after SR59230A treatment (Fig. 7B, left). The qPCR results also indicated that the level of mitochondrial biogenetic gene Nrf1 was downregulated after SR59230A treatment while the change had no statistical significance (Fig. 7B, right). In agreement with the result, sWAT collected from VEGF-A Tg mice upon treatment with SR59230 consistently exhibited a lower oxygen consumption rate (OCR) than the vehicle-treated VEGF-A Tg mice at different time points upon treatment with different compounds (Fig. 7C, compare the blue and red curves).

Collectively, our results suggest that the β3-AR signaling pathway is necessary and sufficient for the VEGF-A-induced metabolic effects in adipose tissue.

Based on these results, we present a working model (Fig. 8). According to the model, adipose tissue-derived VEGF-A stimulates sympathetic innervation in adipose tissue. NE, locally released by the stimulated sympathetic nerve fibers, triggers the activation of β3-AR signaling, which in turn induces higher levels of cAMP, resulting in activation of PKA. The activated PKA phosphorylates the rate-limiting lipolytic enzyme HSL and promotes lipolysis in adipocytes. Furthermore, PKA phosphorylates critical transcriptional factors which directly upregulate the expression of UCP1 and browning in sWAT (27, 28). Both lipolysis and browning facilitate the lipid breakdown as well as heat generation in mitochondria, which ultimately results in enhanced energy expenditure.

DISCUSSION

In response to overnutrition stress, adipose tissue expands with rapid speed, and the blood vessels cannot keep pace with the expansion (1). Local hypoxia thus develops. The hypoxic microenvironment in the obese adipose tissue may lead to fibrosis and inflammation, which further causes systemic insulin resistance (4, 29, 30). Previously, we along with others reported that overexpression of VEGF-A in adipose tissue may counteract all of these adverse effects by inducing angiogenesis and increasing energy expenditure, both of which bring about metabolic improvement in the diet-induced obese mice (11, 13–16, 18). Among these reports, the most exciting finding is that in addition to directly activating BAT, VEGF-A stimulates a BAT-like phenotype (browning effect) in sWAT of the transgenic mice (11, 13, 14). In the current study, we identified

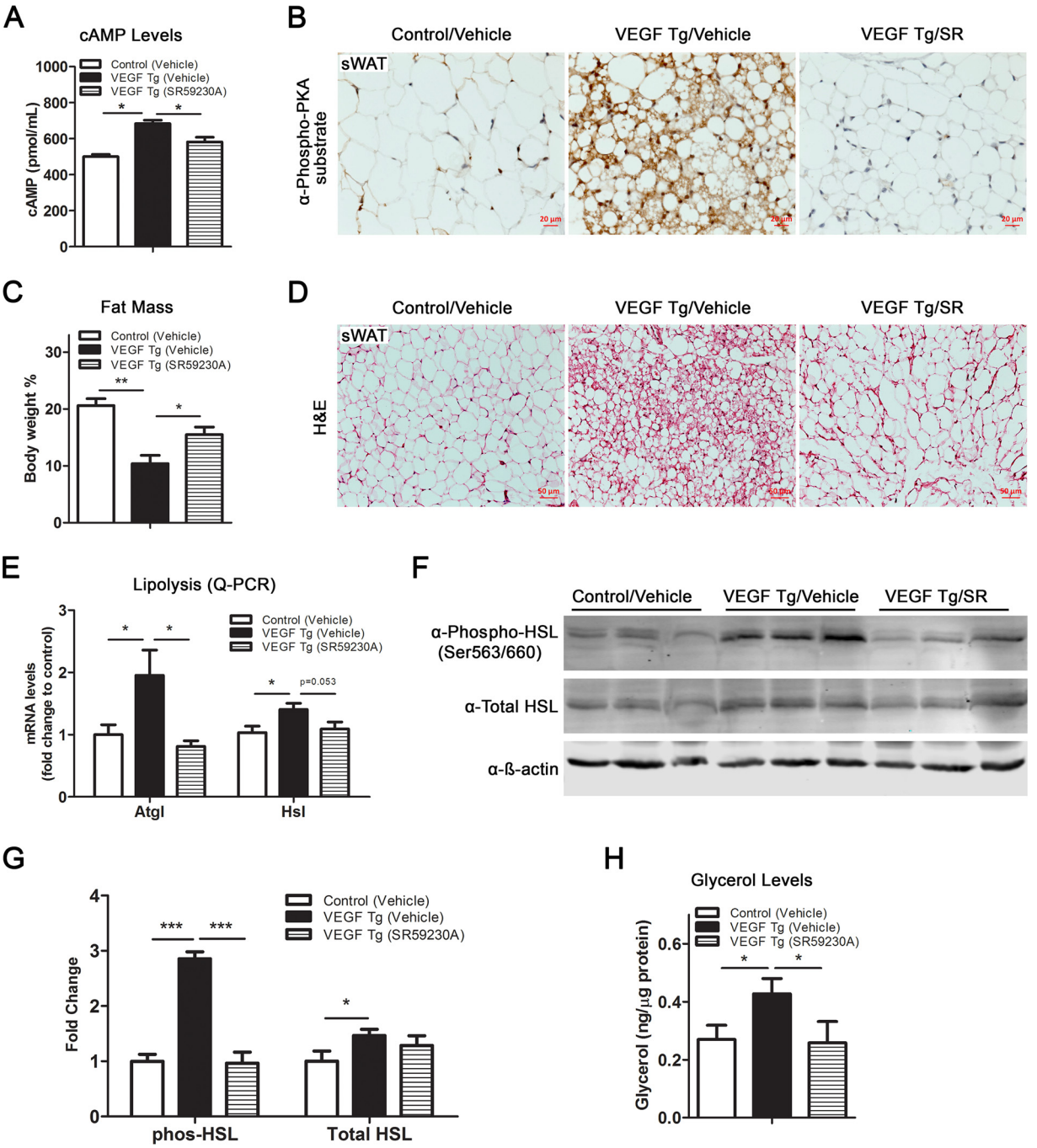

FIG 6 SR59230A, a selective β3-AR antagonist, suppresses VEGF-A-induced lipolysis in sWAT. (A) cAMP levels in sWAT of VEGF Tg mice and their littermate controls after HFD-Dox feeding, with or without SR59230A treatment, for 7 days ($n = 4$ for control group and $n = 5$ for VEGF Tg group; Student's t test, *, $P < 0.05$). (B) IHC staining with anti-phospho-PKA substrate antibody in the sWAT of VEGF Tg mice and their littermate controls after HFD-Dox feeding, with or without SR59230A (SR) treatment, for 7 days (scale bar, 20 μm). (C) MRI analysis of fat mass in VEGF Tg mice and their littermate controls after HFD-Dox feeding, with or without SR59230A treatment, for 7 days. Fat mass was normalized with total body mass ($n = 6$ per group; Student's t test, *, $P < 0.05$; **, $P < 0.01$). (D) H&E staining of sWAT from VEGF Tg mice and their littermate controls after HFD-Dox feeding, with or without SR59230A treatment, for 7 days (scale bar, 50 μm). (E) qPCR analysis of lipolytic genes, namely, *Atgl* and *Hsl*, in sWAT of VEGF Tg mice and their littermate controls after HFD-Dox feeding, with or without SR59230A treatment, for 7 days ($n = 5$ per group; Student's t test, *, $P < 0.05$). (F and G) Western blotting and quantitative measurement of band density on the Western blots by ImageJ software for phosphorylated HSL at serine 563/660 as well as total HSL levels in sWAT of VEGF Tg mice and their littermate controls after HFD-Dox feeding, with or without SR59230A treatment, for 7 days. Results were normalized with β-actin ($n = 3$ per group; Student's t test, *, $P < 0.05$; ***, $P < 0.001$). (H) Glycerol levels in sWAT of VEGF Tg mice and their littermate controls after HFD-Dox feeding, with or without SR59230A treatment, for 7 days ($n = 4$ for control group and $n = 5$ for VEGF Tg group; Student's t test, *, $P < 0.05$).

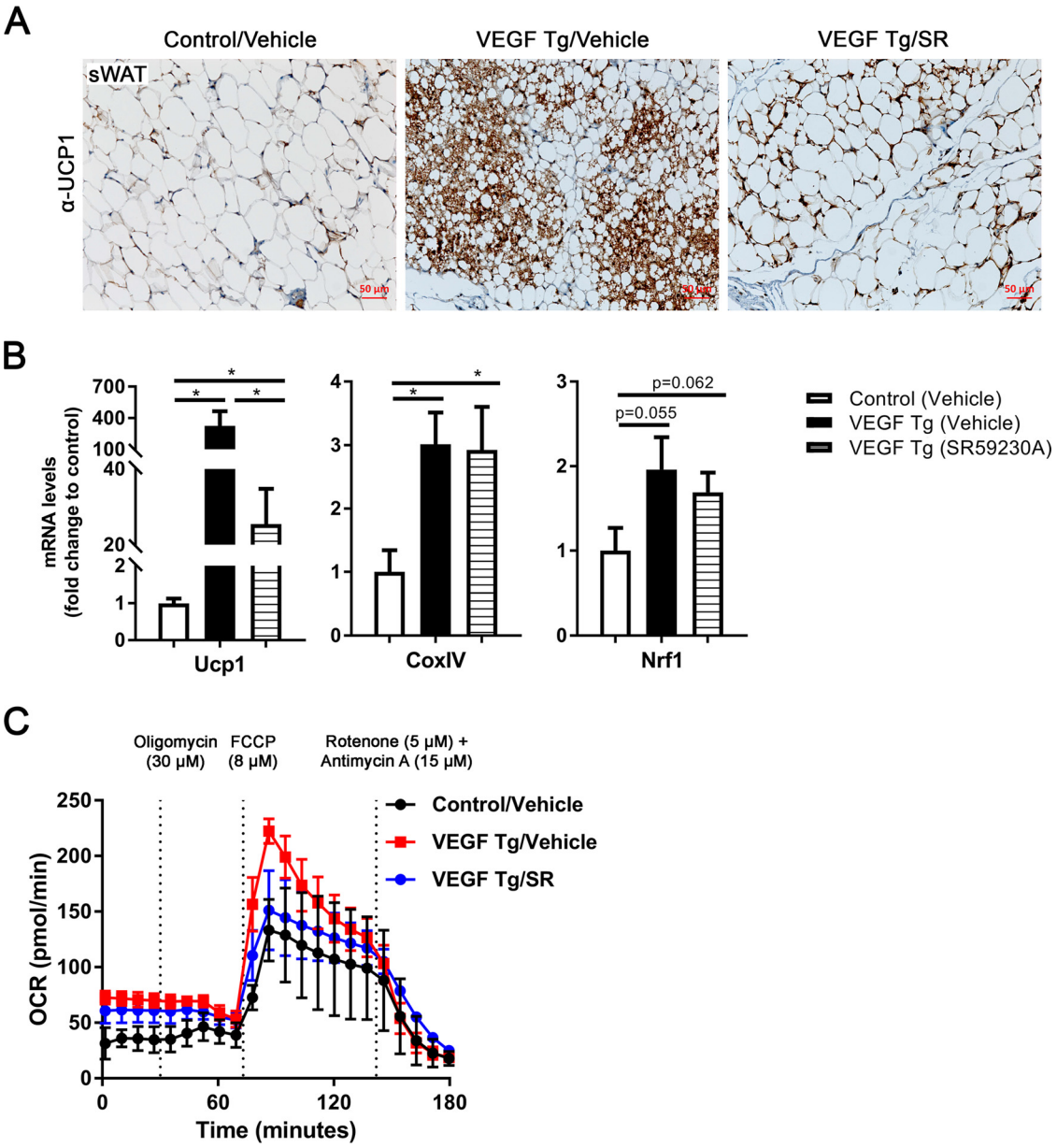

FIG 7 SR59230A suppresses VEGF-A-induced UCP1 expression and mitochondrial function in sWAT. (A) IHC staining with anti-UCP1 antibody in sWAT of VEGF Tg mice and their littermate controls after HFD-Dox feeding, with or without SR59230A (SR) treatment, for 7 days (scale bar, 50 μm). (B) qPCR analysis of *Ucp1* and mitochondrial biogenetic genes including CoxIV and *Nrf1* in sWAT of VEGF Tg mice and their littermate controls after HFD-Dox feeding, with or without SR59230A treatment, for 7 days ($n = 5$ per group; Student's *t* test, *, $P < 0.05$). (C) Oxygen consumption rate (OCR) in sWAT measured by a Seahorse instrument. The sWAT was collected from VEGF Tg mice and their littermate controls after HFD-Dox feeding, with or without SR59230A treatment, for 7 days. The injection time point and final concentration of different compounds used for mitochondrial stress assay are indicated in the panel ($n = 5$ per group).

the mechanism by which adipocyte-derived VEGF-A promotes lipolysis as well as mitochondrial biogenesis and function in both sWAT and BAT. These new findings, together with the browning effect and BAT activation that we previously reported (13, 14), clearly explain enhanced energy expenditure in VEGF-A Tg mice. Importantly, the current study further demonstrates that the effects are caused by activation of the sympathetic tone locally in VEGF-A-overexpressing adipose tissues.

Of note, while we along with numerous others have previously reported metabolically beneficial effects brought about by VEGF-A in adipose tissues, most of these phenomena were observed in obese mice under HFD feeding for at least 5 weeks (11,

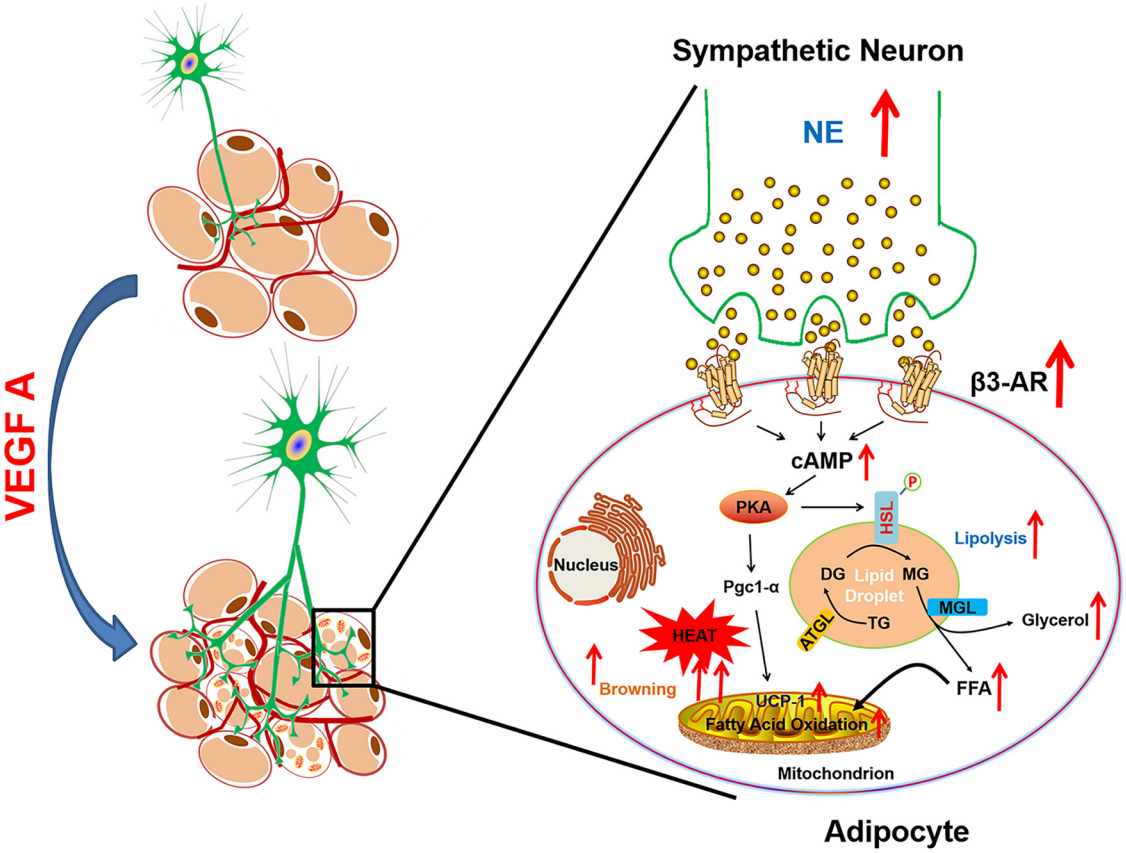

FIG 8 Working model for the functions of VEGF-A in adipose tissue. Adipose-derived VEGF-A stimulates activation of the sympathetic nervous system, which in turn promotes lipolysis and browning, ultimately leading to enhanced energy expenditure. DG, diacylglycerol; TG, triacylglycerol; MG, monoacylglycerol; MGL, monoglyceride lipase; FFA, free fatty acid; ATGL, adipose triglyceride lipase.

14–16). Even though the chronic diet-induced obese mouse models are suitable for studies on the antiobesity effects of VEGF-A, the additional factors that develop during obesity might make it difficult to investigate whether the functions of adipose VEGF-A are direct or indirect. Here, to address the direct effects of VEGF-A in adipose tissue, we took advantage of the Dox-inducible VEGF-A overexpression mouse model and induced VEGF-A expression for only 1 week under HFD feeding. Surprisingly, we found that even after the short period of VEGF-A induction, the transgenic mice showed a dramatic phenotype of metabolic improvement, including smaller body weight gains and enhanced energy expenditure. Of note, the angiogenic and sympathetic innervation effects started after 1 day while the UCP1 upregulation initiated after 2 days of VEGF-A induction. This suggests that adipocyte browning is not an indirect effect of vasculature remodeling but, rather, a result of direct VEGF-A signaling in adipose tissue. The browning effect could be brought about by VEGF-A-stimulated angiogenesis and sympathetic innervation. Notably, all the effects were very minor in eWAT compared to those in sWAT and BAT of VEGF-A Tg mice. The heterogeneity of adipose tissues has also been reported by many others, and it warrants further investigations (31).

A growing body of research has demonstrated that nutrient excess leads to mitochondrial dysfunction (32). For example, obese individuals have been found to have fewer and smaller mitochondria with structural abnormities and reduced oxidative activity. Moreover, the mitochondrial DNA (mtDNA) levels are reduced in the adipose tissue, also supporting a reduction in mitochondrion content and function in obesity (33). These pathological changes dramatically impair the ability of mitochondria to oxidize free fatty acids for use as energy, which causes the adipose tissue to store lipids for fuel instead of burning it. Interestingly, VEGF-A triggered mitochondrial biogenesis

and bioenergetics shortly after induction in the transgenic adipose tissues, as demonstrated by upregulated mitochondrial biogenetic and β-oxidation-related genes as well as by more mtDNA content, increased mitochondrial density, and enhanced OCR. So, how does VEGF-A have the beneficial effects on mitochondrion biogenesis and function? One explanation is that in the diet-induced obese adipose tissue, local hypoxia due to the lack of vasculature shapes an unhealthy microenvironment, which in turn leads to abnormal mitochondrial functions (1, 14). Adipose-derived VEGF-A stimulates functional blood vessel formation which thus suppresses the hypoxic conditions by providing adequate oxygen and nutrients (4, 14). Of high interest in this context is that VEGF-A stimulated massive upregulation of PGC-1α, the primary transcriptional cofactor in the cells which serves as the key driver for mitochondrial biogenesis and function, thereby explaining improved mitochondrial biogenesis and function under HFD challenge. Further studies are needed to identify a more detailed molecular mechanism(s) by which VEGF-A stimulates mitochondrial production and function, especially the critical role of nervous innervation in the process.

While sympathetic nerve fiber innervation in adipose tissue is known to be important for the thermogenic function of BAT/beige adipocytes (34), SNS changes during adipose tissue remodeling have not been explored. Recently, the enriched sympathetic nerve fibers as well as neuro-adipose junctions have been observed by using intravital two-photon microscopy (22, 35). Importantly, Zeng et al. further demonstrated that local optogenetic stimulation of the sympathetic fibers induced lipolysis and browning, which in turn decrease the fat mass (22, 35). They further demonstrated that the lipolytic effect of leptin is via the β-adrenergic signaling pathway (22). Here, for the first time we showed that VEGF-A stimulates the enhancement of innervation in both sWAT and BAT. We further demonstrated that the sympathetic pathway plays essential roles in lipolysis and browning in the VEGF-A transgenic mice. Particularly, we found that the density of sympathetic nerve fibers was significantly enhanced, as indicated by the IF staining of TH, the marker of sympathetic neurons in both WAT and BAT of the transgenic mice. The local NE levels were increased, and the expression of β3-AR was dramatically upregulated in adipose tissues. As a result, the levels of cAMP were increased, and the downstream PKA pathway was activated. The involvement of sympathetic innervation and activation, especially the downstream PKA activation, explains the enhanced lipolysis and browning effects in WAT. Indeed, we found that the levels of HSL phosphorylated by PKA, the critical and rate-limiting lipase in the lipolysis process, were markedly increased and that the levels of UCP1, the marker of the beige cells, was massively upregulated on both the mRNA and protein levels (14, 18). Furthermore, we found that the glycerol levels were increased and that the smaller as well as multilocular lipid droplets were present in the sWAT of the VEGF-A transgenic mice. Importantly, both the lipolytic and browning effects were abolished upon β3-adrenoceptor antagonist, SR59230A, treatment. Collectively, we found that VEGF-A stimulates the increases of the sympathetic drive in WAT. Both lipolysis and browning effects are triggered by the stimulation of β3-AR, which in turn efficiently breaks down the lipid content for thermogenesis in adipose tissues. Whether lipolysis is necessary for browning remains to be elucidated.

An important question raised from the study is that if VEGF-A triggers the neuronal innervation in adipose tissue, would it do so by inducing angiogenesis alone, which in turn upregulates other cytokines to potentiate the neuronal effect, or does it directly function on neuronal fibers in the adipose tissues? While previously VEGF-A had been considered to be solely an endothelial mitogen, recent studies demonstrated that VEGF-A has direct action on neurotrophy and neuronal fiber expansion as well as neuroprotection (36, 37). Specifically, Hobson et al. designed an *in vitro* experiment in a silicone sciatic nerve chamber and found that treatment with VEGF-A dramatically increased nerve axon counts as well as nerve cell proliferation and migration and significantly improved the axon function (38). This study supports the possibility that, in our VEGF-A transgenic adipose tissue, VEGF-A directly interacts with the sympathetic neuronal projection and triggers the fiber proliferation which then induces the inner-

vation effect. Further studies on novel angiogenic animal models would help to address this question.

In conclusion, our study demonstrates the direct function of VEGF-A on sympathetic activation, which further promotes lipolysis and browning effects in adipose tissue, eventually leading to enhanced energy expenditure in the diet-induced obese mice. Since obesity has been considered to be associated with low sympathetic activity (39), our findings thus suggest a potential strategy to combat/prevent obesity and its associated morbidities.

MATERIALS AND METHODS

Animals. The adipose-specific doxycycline (Dox)-inducible VEGF-A transgenic (VEGF Tg) mouse model has been described previously (14). Briefly, to generate the double-transgenic mice, TRE-VEGF Tg mice were crossed with adiponectin promoter-driven rtTA transgenic mice (Apn-rtTA). The double-transgenic mouse (Apn-rtTA/TRE-VEGF-A) expresses VEGF-A in response to Dox treatment. All of these mice are bred on a pure C57BL/6J background. All animal experiments were conducted using littermate-controlled male mice; Apn-rtTA Tg mice were used as control mice. All the experiments were started when these mice were 7 weeks old. Mice were housed in cages with a 12-h dark-light cycle with free access to water and regular chow diet, unless otherwise indicated. The animal study protocols were reviewed and approved by the Animal Welfare Committee of University of Texas Health Science Center at Houston, TX.

Treatments of Dox-containing HFD and SR59230A. For all the experiments under the condition of an HFD plus Dox (HFD-Dox feeding), the mice were fed with a paste diet containing 60% calories from fat and 30 mg/kg Dox (Bio-Serv, Flemington, NJ) for 7 days. For the treatment with the selective β3-adrenoceptor antagonist SR59230A, the VEGF Tg mice were i.p. injected with 1 mg/kg body weight of dissolved SR59230A or with 1% dimethyl sulfoxide (DMSO)–phosphate-buffered saline (PBS) placebo every day along with the Dox-containing HFD for 7 days. At day 8, the mice were fasted for 3 h and sacrificed. Tissues and sera were collected for further analyses. SR59230A compound (Sigma-Aldrich, St. Louis, MO) was dissolved in 1% DMSO-PBS buffer.

Body composition and metabolic cage study. Bone-free lean mass, fat mass, and body fluids were measured in the nonanesthetized mice by using an Echo 3-in-1 nuclear magnetic resonance (NMR) Minispec magnetic resonance imaging (MRI) instrument (EchoMRI, Houston, TX). For the indirect calorimetry study, 7 days after HFD-Dox feeding, the VEGF-A Tg mice and their littermate control mice were housed individually in TSE metabolic chambers (TSE Systems, Chesterfield, MO) and maintained on a 12-h dark-light cycle with lights on from 7 a.m. to 7 p.m. All control and VEGF-A Tg mice were fed with HFD plus Dox and water *ad libitum* during the study. Metabolic profiles were recorded continuously for 2 days using a TSE metabolic chamber documentation system. The data of the second day were used for analyses. Statistical analysis and regression plotting were performed in the R programming language with the CalR software, a recently published analytic tool for indirect calorimetry (40).

Histology. The adipose tissues and the livers were immediately collected after the mice were sacrificed and fixed in 10% PBS-buffered formalin (pH 7.4) (Fisher Scientific Company, Kalamazoo, MI) for 48 h. Following paraffin embedding, the tissue sections were stained with hematoxylin and eosin (H&E) (Sigma-Aldrich) using a standard protocol, as described previously (4).

For immunohistochemistry (IHC) staining, sections were probed with primary antibody against phospho-PKA substrate (1:1000; Cell Signaling Technologies, Danvers, MA) or against UCP1 (1:2000; Abcam), followed by biotinylated secondary antibody. Binding of second antibodies was visualized by using diaminobenzidine (DAB) chromogen A (Thermo Fisher Scientific, Sugar Land, TX) (4). Counterstaining was performed with hematoxylin (Sigma-Aldrich). All of the images were acquired with an Axio Scope A1 microscope and/or ZEISS ZEN2 microscope software (Carl Zeiss). For immunofluorescence (IF) staining, sections were stained with a primary antibody against CoxIV (1:500; Cell Signaling Technologies), followed by donkey anti-rabbit Alexa Fluor 488-conjugated or donkey anti-goat Alexa Fluor 647-conjugated secondary antibodies (1.5 μg/ml; Jackson ImmunoResearch Laboratories, West Grove, PA). Nuclei were stained with 4′,6′-diamidino-2-phenylindole (DAPI; 1 μg/ml) (Vector Laboratories, Burlingame, CA). Images were acquired with a Carl Zeiss upright ApoTome Axio Imager Z1 microscope and ZEN2 Core Imaging software.

Whole-mount immunofluorescent staining and confocal microscopy imaging. The whole-mount IF staining for adipose tissues, including WAT and BAT, has been described previously (22). Briefly, mice were euthanized by isoflurane and perfused slowly via intracardiac injection with fresh PBS (pH 7.4), followed by removal of the right atrium to release blood. Adipose tissues were excised and were fixed with fresh 1% PBS-buffered paraformaldehyde (PFA; pH 7.4) (Electron Microscopy Sciences, Hatfield, PA) for 30 min at room temperature with gentle rocking. After three washes with PBS, the tissues were subdivided into 0.5- to 1-cm^3-sized pieces, followed by blocking with 5% bovine serum albumin (BSA) in PBS for 30 min at room temperature with gentle rocking. Tissues were then incubated with anti-tyrosine hydroxylase (anti-TH) primary antibody (1:1,000) (Pel Freez Biologicals, Rogers, AR) or antiendomucin primary antibody (1:1,000) (R&D Research Systems, Minneapolis, MN) overnight at 4°C followed, by donkey anti-rabbit Alexa Fluor 488-conjugated secondary antibody or donkey anti-goat Alexa Fluor 647-conjugated secondary antibody (1.5 μg/ml) (Jackson ImmunoResearch Laboratories). Nuclei were stained with DAPI (1 μg/ml). Images were acquired with a Carl Zeiss upright ApoTome Axio Imager Z1 and ZEN2 Core Imaging software or confocal Leica TCS SP5 microscope and LAS AF software.

TABLE 1 Primer sequences for qPCR

Gene name	Forward primer (5′–3′)	Reverse primer (5′–3′)
18S rRNA	AAGTCCCTGCCCTTTGTACACA	GATCCGAGGGCCTCACTAAAC
Nrf1	TATGGCGGAAGTAATGAAAGACG	CAACGTAAGCTCTGCCTTGTT
Acadl	TCTTTTCCTCGGAGCATGACA	GACCTCTCTACTCACTTCTCCAG
Acadm	AGGGTTTAGTTTTGAGTTGACGG	CCCCGCTTTTGTCATATTCCG
Acads	AGTGGTGCAGGCTTGGATTAC	ACTGAGGGCAAAACAGCCG
Cpt1a	CTCCGCCTGAGCCATGAAG	CACCAGTGATGATGCCATTCT
Cpt2	CAGCACAGCATCGTACCCA	TCCCAATGCCGTTCTCAAAAT
Echs1	TTGTGAACTTGCCATGATGTGT	TGCTCGGGTGAGTCTCTGAG
CoxIV	CTGCCCGGAGTCTGGTAATG	CAGTCAACGTAGGGGGTCATC
Tfam	GGAATGTGGAGCGTGCTAAAA	ACAAGACTGATAGACGAGGGG
Atgl	ACCACCCTTTCCAACATGCTA	GGCAGAGTATAGGGCACCA
Hsl	TGGCACACCATTTTGACCTG	TTGCGGTTAGAAGCCACATAG
Abhd5	TGGTGTCCCACATCTACATCA	CAGCGTCCATATTCTGTTTCCA
Fasn	GGAGGTGGTGATAGCCGGTAT	TGGGTAATCCATAGAGCCCAG
Acc1	GATGAACCATCTCCGTTGGC	GACCCAATTATGAATCGGGAGTG
Cd36	AGATGACGTGGCAAAGAACAG	CCTTGGCTAGATAACGAACTCTG
Adrb3	CCTTGGGCGAAACTGGTTG	GTTGGTGACAGCTAGGTAGCG
Adra2a	CTTTTGCACGTCGTCCATAGT	CGGTGACAATGATGGCCTTGA

Real-time qPCR. Total RNAs were extracted from tissues by TRIzol according to the company's instructions (Invitrogen, La Jolla, CA). The genomic DNAs were removed by DNase I (5 PRIME, Gaithersburg, MD). The total mRNAs were then purified by an RNeasy RNA extraction kit (Qiagen, La Jolla, CA). The quality and quantity of the RNA were determined by a 260/280 ratio using NanoDrop 2000 (Thermo Fisher Scientific). cDNAs were obtained by reverse transcribing 1 μg of total RNAs with an iScript Select cDNA synthesis kit (Bio-Rad Laboratories, Hercules, CA). Quantitative PCRs (qPCRs) were carried out on a Bio-Rad CFX96 instrument (Bio-Rad Laboratories). The primer sequences are listed in Table 1. Results were calculated using the $2^{-\Delta\Delta CT}$ (where C_T is threshold cycle) method, normalized by the 18S rRNA (4).

Western blotting. Total proteins were extracted using cell lysis buffer (25 mM Tris-HCl, 150 mM NaCl, 0.1% Triton X-100, 0.1% Tween 20, and 0.1% SDS, pH 7.4). The protein concentration was measured by a bicinchoninic acid (BCA) assay kit (ThermoFisher Scientific). A total of 30 μg of cell lysates was separated by 10% or 4 to 20% Bis-Tris SDS gels (Invitrogen, Carlsbad, CA) and transferred to polyvinylidene difluoride (PVDF) membrane (EMD Millipore, Billerica, MA). For immunoblotting, the primary antibodies for β-actin (1:2,000; Santa Cruz Biotechnology, Dallas, TX), total HSL, phosphorylated HSL (serine 563/660, PKA-targeted sites), or SDHA (1:1,000; Cell Signaling Technologies) were used for probing, followed by secondary antibodies labeled with infrared dye emitting at 680 nm or 800 nm (Li-Cor Bioscience, Lincoln, NE). The blots were analyzed by Odyssey software (Li-Cor Bioscience). The density of the bands was quantified by ImageJ software (NIH).

Measurement of NE levels. The NE levels in serum were detected and quantified in duplicate by an enzyme-linked immunosorbent assay (ELISA) kit (Labor Diagnostika Nord GmbH & Co. KG, Nordhorn, Germany) according to the manufacturer's instructions. In brief, for the NE levels in adipose tissue, WAT was homogenized by sonication in homogenization buffer (1 N HCl, 0.25 M EDTA, and 1 M $Na_2S_2O_5$), and the supernatants were collected by centrifugation at 4°C for NE analysis after removal of the fat cake at the top. The NE levels were normalized to the total amount of tissue proteins.

Measurement of glycerol production. A total of 100 mg of WAT was homogenized in 500 μl of chilled PBS with proteinase inhibitors (Sigma-Aldrich). Glycerol levels were analyzed by a glycerol assay kit (BioAssay Systems, Hayward, CA) according to the manufacturer's instructions. The levels were normalized to total tissue protein levels.

Measurement of cAMP levels. cAMP levels in adipose tissue or the serum were detected and quantified in duplicate by an ELISA kit (R&D Systems, Minneapolis, MN) according to the manufacturer's instructions. Briefly, for adipose tissue, WAT was homogenized with a tissue homogenizer in chilled 0.1 N HCl at a 1:5 ratio (wt/vol). Supernatants were collected by centrifugation at 4°C and neutralized with 1 N NaOH for analysis.

Measurement of OCR by Seahorse. The oxygen consumption rate (OCR) of adipose tissues was measured in real time by a Seahorse XFe24 Analyzer (Agilent Technologies, Wilmington, DE) as described previously (41–43). Briefly, adipose tissues were excised and washed twice with assay medium (Dulbecco's modified Eagle's medium [DMEM] with 25 mM glucose, pH 7.4). Each adipose tissue was sampled using a 2-mm Harris Uni-Core punch (Electron Microscopy Sciences, Hatfield, PA), resulting in 2 mg of tissue for each punch. Three tissue punches (total of 6 mg of the tissue) from each fat pad were placed into one well of the XFe24 cell culture microplate (Seahorse Bioscience, North Billerica, MA). Five replicates per fat pad were used for the experiment. The following inhibitors were used at different time points: 30 μM oligomycin A, 8 μM carbonyl cyanide-4-(trifluoromethoxy) phenylhydrazone (FCCP), and a mixture of 5 μM antimycin A and 15 μM rotenone. All of the inhibitors were obtained from Sigma-Aldrich. The OCR readings were normalized by the total amount of DNAs.

Measurement of total lipid content in adipose tissue. A total of 300 mg of WAT excised from the mice was immediately transferred to a 1.5-ml Eppendorf tube with 500 μl of PBS (PH 7.4) at room temperature and was homogenized by a MagNA Lyser (Roche Diagnostics, Basel, Switzerland). The

homogenized samples were centrifuged at 6,000 rpm for 15 min at room temperature to remove the cell debris. The lipid layer was collected and weighed. The amount of lipid content was normalized by total DNAs (30).

Mitochondrial DNA assay. A total of 100 mg of WAT was used for nuclear DNA (nuDNA), and mitochondrial DNA (mtDNA) extraction was performed as previously described (44, 45). The copy numbers of mtDNA were calculated as the ratio determined by qPCR of the mtDNA NADH dehydrogenase alpha 1 (NADHA1) gene to the copy numbers of the nuclear lipoprotein lipase (LPL) gene, as previously described (46).

Statistical analysis. All data are represented as means ± standard errors of the means (SEM). Statistical analysis was performed with GraphPad Prism (GraphPad Software, Inc., La Jolla, CA). Student's *t* test was applied for statistical analysis. For the metabolic cage study, the statistical analysis and regression plotting were performed according to instructions (40). Analysis of covariance (ANCOVA) was applied to determine the difference between the groups. A *P* value of less than 0.05 was considered to be statistically significant.

ACKNOWLEDGMENTS

We thank Philipp Scherer at Touchstone Diabetes Center in the University of Texas Medical Science Center at Dallas for providing the VEGF-A transgenic animal model. We thank Zhengmei Mao in the microscopy core of the Institute of Molecular Medicine for assistance on imaging and tissue processing.

This study was supported by National Institutes of Health (NIH) grant R01DK109001 (to K.S.) and the Harry E. Bovay, Jr., Foundation.

We declare that we have no competing financial interests.

REFERENCES

1. Sun K, Kusminski CM, Scherer PE. 2011. Adipose tissue remodeling and obesity. J Clin Invest 121:2094–2101. https://doi.org/10.1172/JCI45887.
2. Rosen ED, Spiegelman BM. 2014. What we talk about when we talk about fat. Cell 156:20–44. https://doi.org/10.1016/j.cell.2013.12.012.
3. Cao Y. 2013. Angiogenesis and vascular functions in modulation of obesity, adipose metabolism, and insulin sensitivity. Cell Metab 18:478–489. https://doi.org/10.1016/j.cmet.2013.08.008.
4. Sun K, Halberg N, Khan M, Magalang UJ, Scherer PE. 2013. Selective inhibition of hypoxia-inducible factor 1α ameliorates adipose tissue dysfunction. Mol Cell Biol 33:904–917. https://doi.org/10.1128/MCB.00951-12.
5. Halberg N, Khan T, Trujillo ME, Wernstedt-Asterholm I, Attie AD, Sherwani S, Wang ZV, Landskroner-Eiger S, Dineen S, Magalang UJ, Brekken RA, Scherer PE. 2009. Hypoxia-inducible factor 1α induces fibrosis and insulin resistance in white adipose tissue. Mol Cell Biol 29:4467–4483. https://doi.org/10.1128/MCB.00192-09.
6. Ye J, Gao Z, Yin J, He Q. 2007. Hypoxia is a potential risk factor for chronic inflammation and adiponectin reduction in adipose tissue of ob/ob and dietary obese mice. Am J Physiol Endocrinol Metab 293:E1118–E1128. https://doi.org/10.1152/ajpendo.00435.2007.
7. Jiang C, Qu A, Matsubara T, Chanturiya T, Jou W, Gavrilova O, Shah YM, Gonzalez FJ. 2011. Disruption of hypoxia-inducible factor 1 in adipocytes improves insulin sensitivity and decreases adiposity in high-fat diet-fed mice. Diabetes 60:2484–2495. https://doi.org/10.2337/db11-0174.
8. Hosogai N, Fukuhara A, Oshima K, Miyata Y, Tanaka S, Segawa K, Furukawa S, Tochino Y, Komuro R, Matsuda M, Shimomura I. 2007. Adipose tissue hypoxia in obesity and its impact on adipocytokine dysregulation. Diabetes 56:901–911. https://doi.org/10.2337/db06-0911.
9. Zhang QX, Magovern CJ, Mack CA, Budenbender KT, Ko W, Rosengart TK. 1997. Vascular endothelial growth factor is the major angiogenic factor in omentum: mechanism of the omentum-mediated angiogenesis. J Surg Res 67:147–154. https://doi.org/10.1006/jsre.1996.4983.
10. Hausman GJ, Richardson RL. 2004. Adipose tissue angiogenesis. J Anim Sci 82:925–934. https://doi.org/10.2527/2004.823925x.
11. During MJ, Liu X, Huang W, Magee D, Slater A, McMurphy T, Wang C, Cao L. 2015. Adipose VEGF links the white-to-brown fat switch with environmental, genetic, and pharmacological stimuli in male mice. Endocrinology 156:2059–2073. https://doi.org/10.1210/en.2014-1905.
12. Xue Y, Petrovic N, Cao R, Larsson O, Lim S, Chen S, Feldmann HM, Liang Z, Zhu Z, Nedergaard J, Cannon B, Cao Y. 2009. Hypoxia-independent angiogenesis in adipose tissues during cold acclimation. Cell Metab 9:99–109. https://doi.org/10.1016/j.cmet.2008.11.009.
13. Sun K, Kusminski CM, Luby-Phelps K, Spurgin SB, An YA, Wang QA, Holland WL, Scherer PE. 2014. Brown adipose tissue derived VEGF-A modulates cold tolerance and energy expenditure. Mol Metab 3:474–483. https://doi.org/10.1016/j.molmet.2014.03.010.
14. Sun K, Wernstedt Asterholm I, Kusminski CM, Bueno AC, Wang ZV, Pollard JW, Brekken RA, Scherer PE. 2012. Dichotomous effects of VEGF-A on adipose tissue dysfunction. Proc Natl Acad Sci U S A 109:5874–5879. https://doi.org/10.1073/pnas.1200447109.
15. Elias I, Franckhauser S, Ferre T, Vila L, Tafuro S, Munoz S, Roca C, Ramos D, Pujol A, Riu E, Ruberte J, Bosch F. 2012. Adipose tissue overexpression of vascular endothelial growth factor protects against diet-induced obesity and insulin resistance. Diabetes 61:1801–1813. https://doi.org/10.2337/db11-0832.
16. Sung HK, Doh KO, Son JE, Park JG, Bae Y, Choi S, Nelson SM, Cowling R, Nagy K, Michael IP, Koh GY, Adamson SL, Pawson T, Nagy A. 2013. Adipose vascular endothelial growth factor regulates metabolic homeostasis through angiogenesis. Cell Metab 17:61–72. https://doi.org/10.1016/j.cmet.2012.12.010.
17. Townsend KL, An D, Lynes MD, Huang TL, Zhang H, Goodyear LJ, Tseng YH. 2013. Increased mitochondrial activity in BMP7-treated brown adipocytes, due to increased CPT1- and CD36-mediated fatty acid uptake. Antioxid Redox Signal 19:243–257. https://doi.org/10.1089/ars.2012.4536.
18. Park J, Kim M, Sun K, An YA, Gu X, Scherer PE. 2017. VEGF-A-expressing adipose tissue shows rapid beiging and enhanced survival after transplantation and confers IL-4-independent metabolic improvements. Diabetes 66:1479–1490. https://doi.org/10.2337/db16-1081.
19. Kersten S. 2001. Mechanisms of nutritional and hormonal regulation of lipogenesis. EMBO Rep 2:282–286. https://doi.org/10.1093/embo-reports/kve071.
20. Xu S, Jay A, Brunaldi K, Huang N, Hamilton JA. 2013. CD36 enhances fatty acid uptake by increasing the rate of intracellular esterification but not transport across the plasma membrane. Biochemistry 52:7254–7261. https://doi.org/10.1021/bi400914c.
21. Lass A, Zimmermann R, Oberer M, Zechner R. 2011. Lipolysis—a highly regulated multi-enzyme complex mediates the catabolism of cellular fat stores. Prog Lipid Res 50:14–27. https://doi.org/10.1016/j.plipres.2010.10.004.
22. Zeng W, Pirzgalska RM, Pereira MM, Kubasova N, Barateiro A, Seixas E, Lu YH, Kozlova A, Voss H, Martins GG, Friedman JM, Domingos AI. 2015. Sympathetic neuro-adipose connections mediate leptin-driven lipolysis. Cell 163:84–94. https://doi.org/10.1016/j.cell.2015.08.055.
23. Harms M, Seale P. 2013. Brown and beige fat: development, function and

therapeutic potential. Nat Med 19:1252–1263. https://doi.org/10.1038/nm.3361.
24. Schulz TJ, Tseng YH. 2013. Systemic control of brown fat thermogenesis: integration of peripheral and central signals. Ann N Y Acad Sci 1302:35–41. https://doi.org/10.1111/nyas.12277.
25. Peirce V, Carobbio S, Vidal-Puig A. 2014. The different shades of fat. Nature 510:76–83. https://doi.org/10.1038/nature13477.
26. Mottillo EP, Granneman JG. 2011. Intracellular fatty acids suppress beta-adrenergic induction of PKA-targeted gene expression in white adipocytes. Am J Physiol Endocrinol Metab 301:E122–E131. https://doi.org/10.1152/ajpendo.00039.2011.
27. Cao W, Daniel KW, Robidoux J, Puigserver P, Medvedev AV, Bai X, Floering LM, Spiegelman BM, Collins S. 2004. p38 mitogen-activated protein kinase is the central regulator of cyclic AMP-dependent transcription of the brown fat uncoupling protein 1 gene. Mol Cell Biol 24:3057–3067. https://doi.org/10.1128/MCB.24.7.3057-3067.2004.
28. Liu D, Bordicchia M, Zhang C, Fang H, Wei W, Li JL, Guilherme A, Guntur K, Czech MP, Collins S. 2016. Activation of mTORC1 is essential for beta-adrenergic stimulation of adipose browning. J Clin Invest 126:1704–1716. https://doi.org/10.1172/JCI83532.
29. Sun K, Tordjman J, Clement K, Scherer PE. 2013. Fibrosis and adipose tissue dysfunction. Cell Metab 18:470–477. https://doi.org/10.1016/j.cmet.2013.06.016.
30. Zhao Y, Gu X, Zhang N, Kolonin MG, An Z, Sun K. 2016. Divergent functions of endotrophin on different cell populations in adipose tissue. Am J Physiol Endocrinol Metab 311:E952–E963. https://doi.org/10.1152/ajpendo.00314.2016.
31. Kwok KH, Lam KS, Xu A. 2016. Heterogeneity of white adipose tissue: molecular basis and clinical implications. Exp Mol Med 48:e215. https://doi.org/10.1038/emm.2016.5.
32. Bournat JC, Brown CW. 2010. Mitochondrial dysfunction in obesity. Curr Opin Endocrinol Diabetes Obes 17:446–452. https://doi.org/10.1097/MED.0b013e32833c3026.
33. Patti ME, Corvera S. 2010. The role of mitochondria in the pathogenesis of type 2 diabetes. Endocr Rev 31:364–395. https://doi.org/10.1210/er.2009-0027.
34. Ramseyer VD, Granneman JG. 2016. Adrenergic regulation of cellular plasticity in brown, beige/brite and white adipose tissues. Adipocyte 5:119–129. https://doi.org/10.1080/21623945.2016.1145846.
35. Jiang H, Ding X, Cao Y, Wang H, Zeng W. 2017. Dense intra-adipose sympathetic arborizations are essential for cold-induced beiging of mouse white adipose tissue. Cell Metab 26:686–692.e3. https://doi.org/10.1016/j.cmet.2017.08.016.
36. Rosenstein JM, Krum JM. 2004. New roles for VEGF in nervous tissue—beyond blood vessels. Exp Neurol 187:246–253.
37. Rosenstein JM, Krum JM, Ruhrberg C. 2010. VEGF in the nervous system. Organogenesis 6:107–114. https://doi.org/10.4161/org.6.2.11687.
38. Hobson MI, Green CJ, Terenghi G. 2000. VEGF enhances intraneural angiogenesis and improves nerve regeneration after axotomy. J Anat 197:591–605. https://doi.org/10.1046/j.1469-7580.2000.19740591.x.
39. Bray GA, York DA. 1998. The MONA LISA hypothesis in the time of leptin. Recent Prog Horm Res 53:95–117.
40. Mina AI, LeClair RA, LeClair KB, Cohen DE, Lantier L, Banks AS. 4 July 2018. CalR: a web-based analysis tool for indirect calorimetry experiments. Cell Metab. https://doi.org/10.1016/j.cmet.2018.06.019.
41. Dunham-Snary KJ, Sandel MW, Westbrook DG, Ballinger SW. 2014. A method for assessing mitochondrial bioenergetics in whole white adipose tissues. Redox Biol 2:656–660. https://doi.org/10.1016/j.redox.2014.04.005.
42. Bugge A, Dib L, Collins S. 2014. Measuring respiratory activity of adipocytes and adipose tissues in real time. Methods Enzymol 538:233–247. https://doi.org/10.1016/B978-0-12-800280-3.00013-X.
43. Calderon-Dominguez M, Alcalá M, Sebastián D, Zorzano A, Viana M, Serra D, Herrero L. 2017. Brown adipose tissue bioenergetics: a new methodological approach. Adv Sci (Weinh) 4:1600274. https://doi.org/10.1002/advs.201600274.
44. Haurogne K, Bach JM, Lieubeau B. 2007. Easy and rapid method of zygosity determination in transgenic mice by SYBR green real-time quantitative PCR with a simple data analysis. Transgenic Res 16:127–131. https://doi.org/10.1007/s11248-006-9024-4.
45. Quispe-Tintaya W, White RR, Popov VN, Vijg J, Maslov AY. 2013. Fast mitochondrial DNA isolation from mammalian cells for next-generation sequencing. Biotechniques 55:133–136. https://doi.org/10.2144/000114077.
46. Lai L, Leone TC, Zechner C, Schaeffer PJ, Kelly SM, Flanagan DP, Medeiros DM, Kovacs A, Kelly DP. 2008. Transcriptional coactivators PGC-1α and PGC-lβ control overlapping programs required for perinatal maturation of the heart. Genes Dev 22:1948–1961. https://doi.org/10.1101/gad.1661708.